HPU2 Journal of Sciences:
Natural Sciences and Technology

Journal homepage: https://sj.hpu2.edu.vn

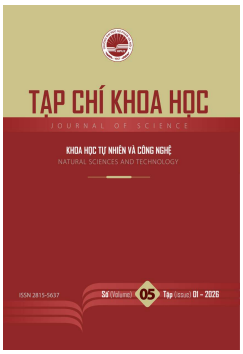

Article type: Research article

Removal of Cr(VI) from aqueous solutions using $MnFe_2O_4$–Coffee husk activated carbon composite

Thuy-Linh Dinh, Thi-Hien Nguyen, Van-Thuan Nguyen, Thuy-Tien Do*

Hanoi Pedagogical University 2, Phu Tho, Vietnam

Abstract

This work reports the fabrication of $MnFe_2O_4$-based composite adsorbents (MFO@CF) derived from HNO_3-activated coffee husk biochar via a combination of co-precipitation and hydrothermal methods. The structural and chemical characteristics of the prepared nanocomposites were analyzed using Scanning Electron Microscopy (SEM) and Fourier Transform Infrared Spectroscopy (FTIR). Batch adsorption experiments were conducted to evaluate the Cr(VI) removal performance under various operational conditions, including solution pH (2÷8), contact time (10÷120 min), and initial Cr(VI) concentration (5÷30 $mg \cdot L^{-1}$). The findings indicate that the MFO@CF composite exhibited effective Cr(VI) removal, which can be attributed to electrostatic interactions and the presence of functional groups on the composite surface. According to the Langmuir isotherm model, the maximum adsorption capacity of MFO@CF reached 30.45 $mg \cdot g^{-1}$, demonstrating its potential as an adsorbent for Cr(VI) removal in wastewater treatment applications. The adsorption kinetics followed a pseudo-second-order model, suggesting that chemisorption may be involved in the adsorption process.

Keywords: $MnFe_2O_4$, Cr(VI), composite materials, coffee husk, activated carbon

1. Introduction

Water contamination by heavy metals, particularly hexavalent chromium (Cr(VI)), poses a significant threat to human health and ecosystems [1]. Cr(VI) is widely detected in industrial effluents, such as electroplating, leather tanning, textile dyeing, and metallurgical processes. Owing to its high toxicity, strong bioaccumulation potential, and carcinogenic properties, Cr(VI) is recognized as a priority

* Corresponding author, E-mail: dothuytien@hpu2.edu.vn

https://doi.org/10.56764/hpu2.jos.2025.5.1.35-44

Received date: 04-3-2026 ; Revised date: 24-3-2026 ; Accepted date: 06-4-2026

hazardous pollutant requiring stringent regulation. However, conventional treatment technologies, such as chemical precipitation, ion exchange, and membrane filtration, frequently present drawbacks, including high operational costs, limited removal efficiency, and poor reusability.

Given this context, the development of novel adsorbent materials with high efficiency, low cost, and eco-friendly sustainability is highly desirable. Although activated carbon is widely used as an adsorbent, its Cr(VI) removal efficiency remains limited [2], [3]. In contrast, $MnFe_2O_4$ magnetic nanoparticles exhibit considerable adsorption capacity and facilitate rapid recovery via an external magnetic field after treatment [4]. A promising strategy involves integrating activated carbon with $MnFe_2O_4$ nanoparticles to develop composite materials that not only enhance pollutant removal performance but also enable facile recovery via an external magnetic field, thereby overcoming the regeneration limitations of conventional adsorbents. $MnFe_2O_4$/activated carbon nanocomposites derived from agricultural by-products can be fabricated through a relatively simple and environmentally benign process. The advantages of this composite arise from the synergistic adsorption effects of activated carbon and $MnFe_2O_4$, along with its favorable thermal stability and structural durability in aqueous environments, which make it highly suitable for environmental remediation applications [5]–[11]. In 2013, Yanzhen Xiao et al. developed an $MnFe_2O_4$/chitosan composite for Cr(VI) removal, achieving an adsorption capacity of 35.2 mg/g [5]. More recently, Wenxiang Jing et al. synthesized a $MnFe_2O_4$-containing bamboo carbon aerogel (MCA), which exhibited high adsorption capacities for Pb^{2+}, Cu^{2+}, and Cd^{2+} (74.38, 84.21, and 73.63 mg/g, respectively), indicating its strong potential for heavy metal removal from wastewater [7]. Additionally, Vatankhah et al. (2024) prepared Mn-doped Fe_2O_4 nanoparticles supported on activated carbon for boron removal, achieving a maximum efficiency of 96.44% under optimal conditions (pH 6.0, adsorbent dosage 0.1 g/L, initial concentration 1 mg/L, and contact time 85 min) [8]. In recent years, research in Vietnam has increasingly focused on the development of nanomaterials for the removal of heavy metal ions (e.g., As, Cr, Pb) and dyes such as methylthioninium chloride (MB). Researchers at Hanoi University of Science and Technology have synthesized GO–Fe_3O_4 and GO–$MnFe_2O_4$ core–shell nanocomposites for the removal of As(V) and MB from aqueous solutions. The GO–Fe_3O_4 composite exhibited a maximum As(V) adsorption capacity of 20.05 mg/g with a removal efficiency of ~99.6% at an equilibrium time of 105 min [9]. In addition, Tran Dai Lam et al. prepared a ferromagnetic iron oxide–chitosan composite via co-precipitation, which showed a high Cr(VI) adsorption capacity of up to 55.8 mg/g [10]. Nevertheless, studies on $MnFe_2O_4$/activated carbon composites derived specifically from coffee husks for environmental treatment remain scarce. The novelty of this study lies in the development of a $MnFe_2O_4$/biochar nanocomposite synthesized from coffee husk-derived biochar, chemically modified with HNO_3 to enhance surface functionality. This approach not only valorizes an abundant agro-industrial by-product but also introduces a sustainable, cost-effective adsorbent with enhanced Cr(VI) adsorption capacity. The nanocomposite was synthesized using a combination of co-precipitation and hydrothermal methods. Its adsorption performance was systematically investigated by examining several key factors, including solution pH, contact time, and the initial concentration of Cr(VI). These experiments enabled the determination of the maximum adsorption capacity of the composite material toward Cr(VI).

2. Materials and Methods

2.1. Chemicals and Instrumentation

The synthesis and evaluation of the $MnFe_2O_4$/biochar nanocomposites utilized the following analytical-grade reagents: manganese(II) chloride tetrahydrate ($MnCl_2 \cdot 4H_2O$, 99%, Merck, Germany), iron(III) chloride hexahydrate ($FeCl_3 \cdot 6H_2O$, 99%, Merck, Germany), nitric acid (HNO_3, 63%), sodium

hydroxide (NaOH, 96%), phosphoric acid (H_3PO_4, 95%), ethanol (Aladdin, China), Potassium dichromate $K_2Cr_2O_7$ (99.8%) (Daejeon, Korea), 1,5-diphenylcarbazide, and deionized water.

The experimental setup included the following instrumentation: a UV-Vis spectrophotometer (Jasco, V-730, Japan) for Cr(VI) concentration analysis, an IKA horizontal shaker for adsorption experiments, a HACH CDC401 handheld pH meter for pH measurements, a centrifuge for phase separation, a laboratory oven for thermal treatments, and an analytical balance for precise mass measurements.

2.2. Synthesis of composite materials

* Preparation of HNO_3-Activated Biochar: Raw coffee husks were cleaned with distilled water, oven-dried at 110 °C for 24 h, and milled to a particle size of 0.5–1.0 mm. The biomass was subsequently soaked in a 3 M HNO_3 solution at 80 °C for 4 h with a solid-to-liquid ratio of 1:10 (10 g biomass:100 mL acid solution). After acid impregnation, the material was thoroughly rinsed with distilled water until a near-neutral pH (7÷8) was achieved and then dried at 70 °C to constant weight. The obtained precursor (10 g) was then carbonized in a porcelain crucible at 350 °C for 60 min under an argon atmosphere with a heating rate of 5 °C min^{-1}, resulting in the formation of HNO_3-activated biochar, denoted as CF.

* Synthesis of $MnFe_2O_4$ (MFO): $MnFe_2O_4$ nanoparticles were synthesized using a co-precipitation method. Specifically, 50 mL of $MnCl_2 \cdot 4H_2O$ solution (0.1 M) and 50 mL of $FeCl_3 \cdot 6H_2O$ solution (0.2 M) were mixed in distilled water in a conical flask to obtain a Mn^{2+}:Fe^{3+} molar ratio of 1:2. The mixture was magnetically stirred for 90 min (Flask 1). Meanwhile, 65 mL of 2 M NaOH solution was prepared in another conical flask (Flask 2). Both solutions were heated to 80 °C in a water bath. Subsequently, the solution in Flask 1 was gradually added to Flask 2 under continuous stirring, and the reaction mixture was maintained at 80 °C for an additional 90 min. The formed precipitate was then filtered, thoroughly washed with distilled water until the filtrate reached a neutral pH (~7), and dried at 80 °C for 24 h to obtain $MnFe_2O_4$ nanoparticles (MFO).

* Synthesis of $MnFe_2O_4$/Activated carbon Nanocomposites (MFO@CF): $MnFe_2O_4$/activated carbon nanocomposites were synthesized by combining $MnFe_2O_4$ (MFO) with CF at a mass ratio of 1:3 (MFO:activated carbon). The mixture was dispersed in 70 mL of double-distilled water in a conical flask and magnetically stirred for 3 h to obtain a homogeneous suspension. The resulting suspension was then transferred into Teflon-lined stainless-steel autoclaves and subjected to hydrothermal treatment at 200 °C for 12 h. After naturally cooling to room temperature, the products were collected by centrifugation, thoroughly washed with distilled water until the supernatant reached neutral pH (~7), and finally dried at 80 °C until constant weight [9].

2.3. Adsorption experiments

The Cr(VI) adsorption behavior of the MFO@CF composite was systematically examined by varying several operational parameters, namely solution pH (2÷8), contact time (10÷120 min), and the initial Cr(VI) concentration (5÷30 mg·L^{-1}). For control experiments, the Cr(VI) concentration was maintained at 10 mg·L^{-1}. Batch adsorption experiments were performed in 250 mL beakers with constant shaking at 120 rpm using an IKA horizontal shaker at ambient temperature (25 ± 2 °C). Following adsorption, the mixtures were allowed to settle and then filtered to separate the adsorbent from the solution. The residual concentration of Cr(VI) in the filtrate was measured using a UV–Vis spectrophotometer (Model 730, Japan) at 540 nm. Concentration values were obtained from a previously established calibration curve ($y = 0.5975x + 0.019$, $R^2 = 0.9996$). Each experiment was repeated three times, and the average results were reported.

The adsorption capacity (q_e, mg g^{-1}) and removal efficiency (H, %) were calculated according to the following equations: $q_e = \frac{(C_o - C_e)V}{m}$ (1); $H = \frac{(C_o - C_e)}{C_o} \times 100\%$ (2)

Where: q_e: adsorption capacity of the material (mg·g^{-1}); C_o: initial Cr(VI) concentration (mg·L^{-1}); C_e: equilibrium concentration of Cr(VI) in the solution (mg·L^{-1}); V: volume of solution (L); m: mass of material (g).

All experimental data were processed using Microsoft Excel, whereas adsorption isotherm fitting and kinetic modeling were performed with Origin 2026 software. The graphical results are presented as the average values accompanied by their standard deviations (mean ± SD).

3. Results and discussion

3.1. The surface structure of the material

The morphological characteristics of the synthesized materials were examined via Scanning Electron Microscopy (SEM, Hitachi S-4800), with representative images presented in Figure 1. The pristine biochar derived from coffee husks exhibits a fibrous architecture characterized by elongated, densely packed fibers with a relatively smooth surface and minimal porosity (Figure 1a). This structure is typical of lignocellulosic biomass, indicating its inherent cellular structure [12]. Further modification with 3 M HNO_3 results in the CF biochar, which exhibits a highly porous structure with well-distributed micropores and mesopores, accompanied by a smoother surface texture (Figure 1b). The HNO_3 activation process introduces oxygen-containing functional groups [13] and enhances pore development through oxidative etching, significantly altering the surface morphology and improving the material's adsorption potential. The MFO@CF composite (Figure 1c) displays a highly porous surface dominated by rod-like structures interspersed with multiple pores, where individual $MnFe_2O_4$ nanoparticles are less distinctly discernible. This morphology suggests a more integrated composite structure, potentially resulting from stronger chemical interactions between the HNO_3-activated biochar's oxygen-rich functional groups and the $MnFe_2O_4$ nanoparticles during hydrothermal treatment [14]. The rod-like structures may arise from the biochar surface reorganization under acidic conditions, facilitating the formation of a more compact and porous hybrid material.

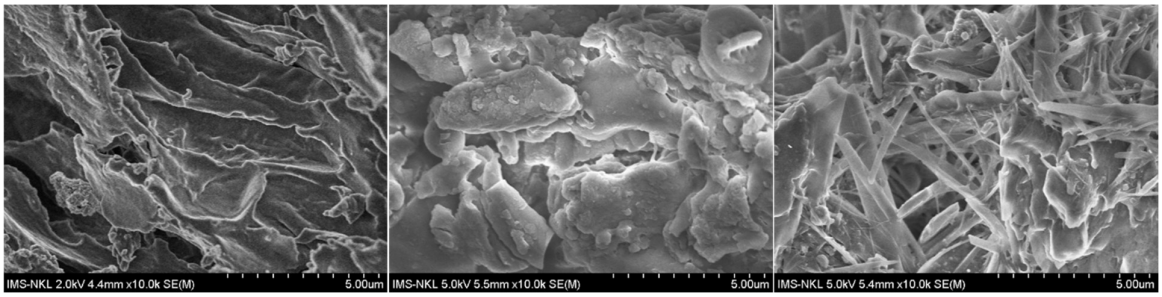

Figure 1. The SEM images of biochar **a)**, activated carbon **b)** and MFO@CF **c)**.

Figure 2 illustrates the FTIR spectra of biochar, activated carbon, and the MFO@CF composite, highlighting differences in their surface functional groups. In the spectrum of biochar, absorption bands at 3647 and 3116 cm^{-1} correspond to O–H stretching vibrations [15], whereas the band at 1446 cm^{-1} is associated with C–O stretching vibrations [16]. These oxygen-containing functional groups are typically formed during the thermal oxidation of coffee husk biomass. Comparable O–H and C–O groups were also

observed in the MFO@CF composite, although their characteristic bands exhibited noticeable shifts relative to those of activated carbon. Specifically, the O–H stretching band shifted from 3647 to 3425 cm^{-1}, and the C–O band moved from 1446 to 1384 cm^{-1} after composite formation. Furthermore, the appearance of a peak at 578 cm^{-1}, attributed to Mn–Fe–O vibrations [17], verifies the successful incorporation of the spinel ferrite phase into the composite.

The point of zero charge (pH_{PZC}), often referred to as the isoelectric point, corresponds to the pH at which the overall surface charge of a material is neutral. At solution pH values below the pH_{PZC}, the material surface becomes positively charged, which enhances the attraction of anionic species. Conversely, when the pH of the solution is higher than the pH_{PZC}, the surface acquires a negative charge, favoring the adsorption of cationic species [18]. As presented in Figure 3, the pH_{PZC} of the MFO@CF composite was found to be 3.45, indicating the acidic nature of the material surface. Knowledge of the pH_{PZC} is essential for determining the appropriate pH conditions for Cr(VI) adsorption by the composite material.

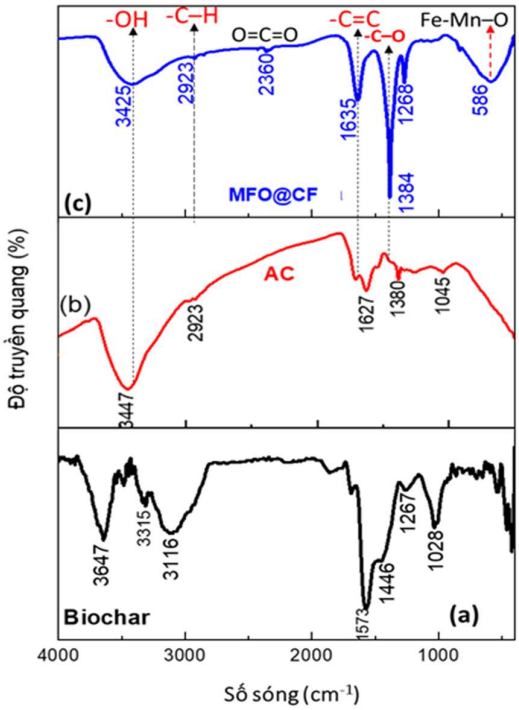

Figure 2. FTIR spectrum of biochar (a), activated carbon (b) and MFO@CF (c).

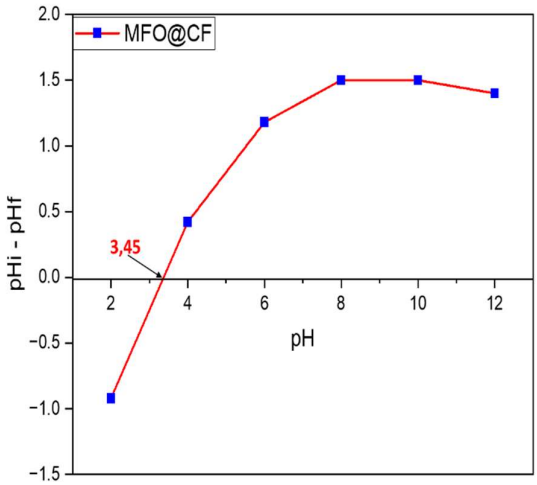

Figure 3. pH_{PZC} of MFO@CF.

3.2. Effect of operating parameters on Cr(VI) adsorption by MFO@CF

3.2.1. Effect of solution pH on Cr(VI) adsorption by MFO@CF

Figure 4 shows the influence of solution pH on the adsorption performance of MFO@CF toward Cr(VI). The maximum adsorption capacity was obtained at pH 2, where the value of q reached 11.46 $mg \cdot g^{-1}$ with a removal efficiency of 64.9%. A slight decrease in adsorption was observed as the pH increased from 2 to 3, followed by a more pronounced reduction when the pH increased further from 4 to 8.

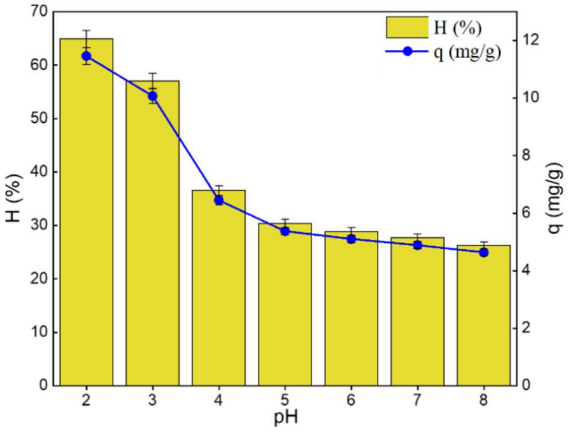

Figure 4. Effect of solution pH on Cr(VI) adsorption capacity (t = 60 min, adsorbent dosage = 1 g·L^{-1}, C_o = 10 mg·L^{-1}).

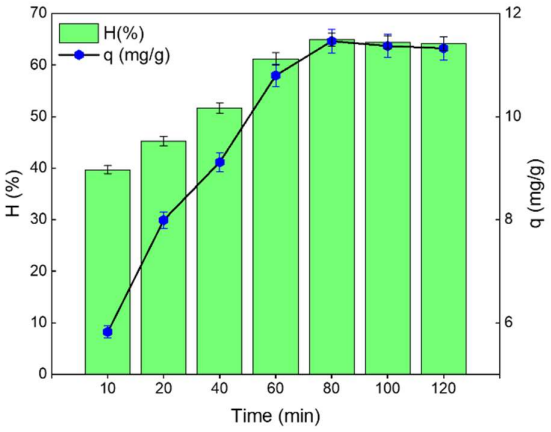

Figure 5. Effect of time on Cr(VI) adsorption capacity (pH = 2, adsorbent dosage = 1 g·L^{-1}, C_o = 10 mg·L^{-1}).

This trend is closely related to both Cr(VI) speciation in aqueous solution and the surface charge properties of the adsorbent. Under the investigated pH range (2÷8) and concentration range (5÷10 mg·L^{-1}), Cr(VI) predominantly exists as the anionic species $HCrO_4^-$ and CrO_4^{2-} [19]. According to the pH_{PZC} value of MFO@CF (3.45, Figure 3), the surface of the composite becomes negatively charged at pH values higher than this point. In contrast, at pH values below the pH_{PZC}, surface functional groups such as –OH and –COOH become protonated, generating positively charged sites that facilitate the adsorption of anionic chromium species. The adsorption mechanism of the MFO@CF is primarily governed by electrostatic attraction and pore-filling effects. The electrostatic interaction between MFO@CF and Cr(VI) species plays a dominant role in the adsorption process. At lower pH values, the concentration of H^+ ions increases, enhancing surface protonation and strengthening electrostatic attraction, thereby improving the adsorption capacity. Therefore, pH 2 was selected as the optimal condition for subsequent experiments.

3.2.2. Effect of contact time on Cr(VI) adsorption capacity

Figure 5 presents the effect of contact time on the adsorption performance of the MFO@CF composite for Cr(VI) removal. A rapid increase in adsorption capacity was observed during the first 10÷80 min, where the value of q rose from 8 to 11.46 mg·g^{-1}, accompanied by an increase in removal efficiency from 45.26% to 64.93%. Beyond 80 min, the adsorption rate slowed and the capacity remained nearly unchanged until 120 min, indicating that the adsorption process had reached equilibrium. At this equilibrium time (80 min), the adsorption capacity of MFO@CF was 11.46 mg·g^{-1} with a removal efficiency of 64.93%. Consequently, 80 min was selected as the optimal contact time for subsequent experiments.

Adsorption kinetics studies:

The adsorption kinetics were analyzed using two common kinetic models, namely the pseudo-first-order [20] and pseudo-second-order models [21]. These models are mathematically represented by Equations (3), and (4), respectively

$$\ln (q_e - q_t) = lnq_e - k_1 t \quad (3)$$

$$\frac{t}{q_t} = \frac{1}{k_2 q_e^2} + \frac{t}{q_e} t \quad (4)$$

where q_t (mg·g^{-1}) and q_e (mg·g^{-1}) represent the adsorption capacities at time t (min) and at equilibrium, respectively. The parameters k_1 (min^{-1}) and k_2 (g·mg^{-1}·min^{-1}) denote the rate constants for the pseudo-first-order and pseudo-second-order kinetic models, respectively.

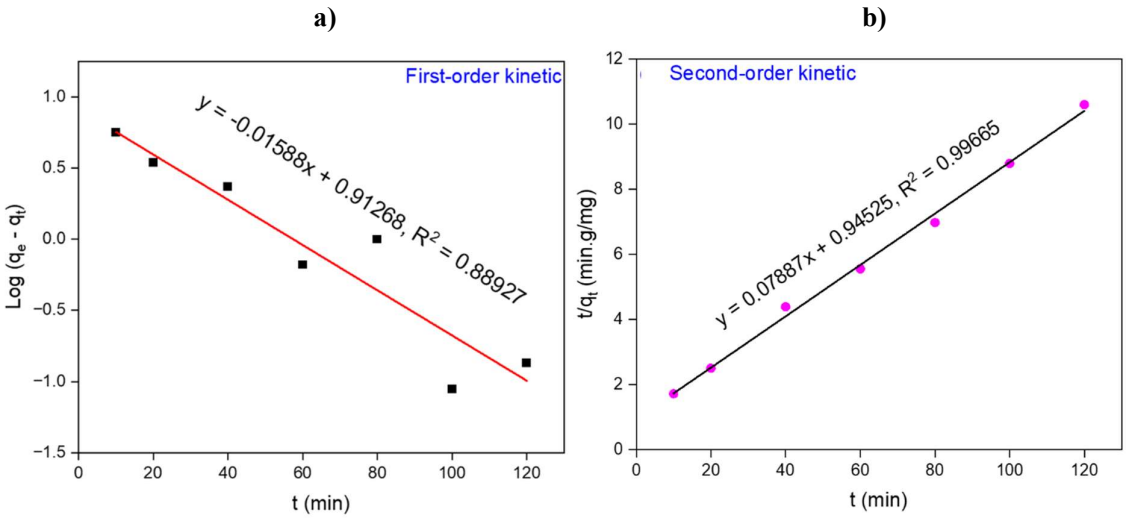

Figure 6. Linear first-order **a)**, and second-order **b)** adsorption kinetics equations for Cr(VI) adsorption of MFO@CF composites.

The adsorption kinetics of Cr(VI) on the MFO@CF composite were evaluated by fitting the experimental data obtained from the contact time experiments to both pseudo-first-order and pseudo-second-order kinetic models. The fitted parameters are summarized in Figure 6 and Table 1.

The correlation coefficient (R^2) for the pseudo-second-order model (0.99665) is significantly higher than that of the pseudo-first-order model (0.88927), indicating that the pseudo-second-order model better describes the adsorption behavior of Cr(VI) on MFO@CF. Moreover, the equilibrium adsorption capacity predicted by this model (q_e = 12.67 mg·g^{-1}) is very close to the experimentally observed value (q_e,exp = 11.46 mg·g^{-1}).

These findings demonstrate that the adsorption kinetics are well described by the pseudo-second-order model, suggesting that chemisorption may be involved in the adsorption process. However, this model alone is not sufficient to conclusively determine the adsorption mechanism. In this study, electrostatic interactions are also likely to play an important role, particularly under acidic conditions. As adsorption progresses and active sites become progressively occupied, the adsorption rate gradually decreases until equilibrium is reached.

Table 1. Kinetic model parameters for Cr(VI) adsorption onto MFO@CF.

First-order kinetic model			**Second-order kinetic model**			$q_{e,exp}$ (mg·g^{-1})
$q_{m,cal}$ (mg·g^{-1})	k_1 (min^{-1})	R^2	$q_{m,cal}$ (mg·g^{-1})	k_2 (g·mg^{-1}·min^{-1})	R^2	11.46
8.18	0.0366	0.8893	12.67	0.0065	0.9966	

3.2.3. Effect of initial Cr(VI) concentration

As presented in Figure 7, an increase in the initial Cr(VI) concentration resulted in a decrease in removal efficiency, while the adsorption capacity of MFO@CF increased. This trend can be explained by the higher driving force for mass transfer at elevated solute concentrations, which enhances the interaction between Cr(VI) ions and the available adsorption sites. These observations are consistent with the theoretical relationships described in Eqs. (1) and (2).

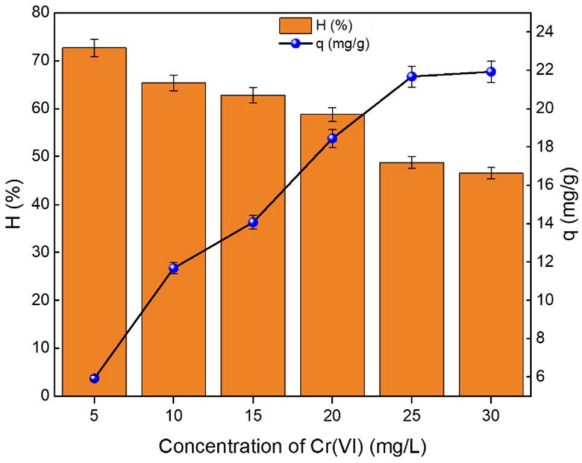

Figure 7. Effect of Cr(VI) concentrations (pH = 2, t = 80 min, adsorbent dosage = 1 g·L^{-1}).

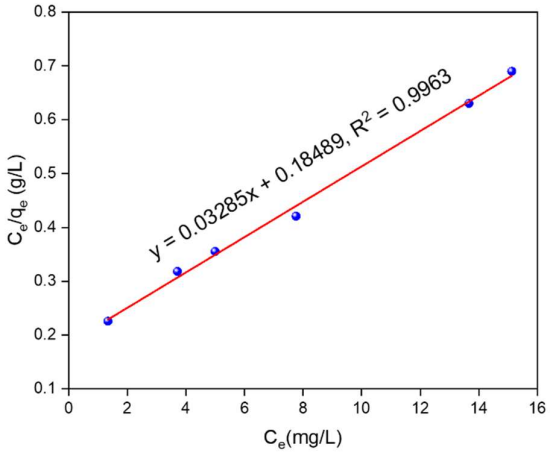

Figure 8. C_e/q_e dependence on C_e for Cr(VI).

Adsorption isotherms are commonly used to describe the equilibrium distribution of adsorbate molecules between the liquid phase and the surface of the adsorbent. Among the various models, the Langmuir isotherm is widely applied to adsorption processes in aqueous systems because it assumes monolayer adsorption on a homogeneous surface with a finite number of active sites [22]. The linear form of the Langmuir equation can be expressed as: $\frac{C_e}{q} = \frac{1}{q_m} C_e + \frac{1}{q_m * b}$ (5).

where C_e represents the equilibrium concentration of Cr(VI) in solution (mg·L^{-1}), q is the adsorption capacity of the adsorbent (mg·g^{-1}), q_m is the maximum adsorption capacity (mg·g^{-1}), and b is the Langmuir constant related to the affinity of the adsorption sites.

Based on the linear plot shown in Figure 8, the maximum adsorption capacity (q_m) was calculated from the slope of the regression line, : $q_m = \frac{1}{tan\ \alpha} = \frac{1}{0.03285}$ = 30.45 (mg·g^{-1}). The obtained value of q_m was 30.45 mg·g^{-1}, indicating that the MFO@CF composite exhibits a considerable adsorption capacity for Cr(VI). The Langmuir constant b was determined to be 0.18

Compared with similar composite materials, the MFO@CF sample demonstrated a higher Cr(VI) adsorption capacity than other adsorbents, such as Magnetic Nanoparticles (q_m = 3.56 mg·g^{-1}) [23], $MnFe_2O_4$@SiO_2 (q_m = 25.04 mg·g^{-1}) [24], and Magnetic activated carbon from animal bone waste (q_m = 27.86 mg·g^{-1}) [25]. In addition, the proposed material achieved comparable performance while requiring a smaller amount of adsorbent and a shorter equilibrium time than other reported adsorbents.

4. Conclusion

In this study, a magnetic composite consisting of $MnFe_2O_4$ nanoparticles and activated carbon derived from coffee husks (MFO@CF) was successfully synthesized through combined co-precipitation and hydrothermal methods. The adsorption performance of the composite toward Cr(VI) in aqueous solution was systematically evaluated by examining the effects of solution pH, contact time, and initial Cr(VI) concentration. The results showed that the adsorption efficiency strongly depended on these operational parameters. Under the optimal conditions (pH = 2, contact time = 80 min, and adsorbent dosage = 1 g·L^{-1}), the maximum adsorption capacity of the MFO@CF composite reached 30.45 mg·g^{-1}. The adsorption process follows the pseudo-second-order model, suggesting that chemisorption may be

involved in the adsorption process. However, electrostatic interactions are also likely to play a significant role, especially under acidic conditions. Compared with previously reported adsorbents, the MFO@CF composite exhibited competitive adsorption performance for Cr(VI) removal. These findings demonstrate that the synthesized material has significant potential as an efficient adsorbent for the treatment of chromium-contaminated wastewater.

Acknowledgments

This research is funded by Hanoi Pedagogical University 2 Foundation for Sciences and Technology Development under Grant Number: SV.2025.HPU2.03.

References

[1] A. Ahmadi, R. Foroutan, H. Esmaeili, and S. Tamjidi, "The role of bentonite clay and bentonite clay@$MnFe_2O_4$ composite and their physico-chemical properties on the removal of Cr(III) and Cr(VI) from aqueous media," *Environ. Sci. Pollut. Res.,* vol. 27, no. 12, pp. 14044–14057, 2020, doi: 10.1007/s11356-020-07756-x.

[2] A. Habineza, J. Zhai, T. Ntakirutimana, F. P. Qiu, X. Li, Q. Wang, "Heavy metal removal from wastewaters by agricultural waste low-cost adsorbents: hindrances of adsorption technology to the large scale industrial application – a review," *Desalin. Water Treat.*, vol. 78, pp. 192–214, 2017, doi: 10.5004/dwt.2017.20581.

[3] A. Othmani, S. Magdouli, P. S. Kumar, A. Kapoor, P. V. Chellam, Ö. Gökkuş, **"**Agricultural waste materials for adsorptive removal of phenols, chromium (VI) and cadmium (II) from wastewater: A review," *Environ. Res.,* vol. 204, Part A, pp. 111916, Mar. 2022, doi: 10.1016/j.envres.2021.111916.

[4] F. Liao, G. Diao, H. Li, "Green synthesis of graphene oxide-$MnFe_2O_4$ composites and their application in removing heavy metal ions," *Micro Nano Lett.*, vol. 15, no. 1, pp. 7–12, Oct. 2019, doi: 10.1049/mnl.2018.5640.

[5] Y. Xiao, H. Liang, and Z. Wang, "$MnFe_2O_4$/chitosan nanocomposites as a recyclable adsorbent for the removal of hexavalent chromium," *Mater. Res. Bull.*, vol. 48, no. 10, pp. 3910–3915, 2013, doi: 10.1016/j.materresbull.2013.05.099.

[6] Y. A. Teymur, F. Güzel & F. Koyuncu, "Adsorptive performance of new Mn-Fe@activated carbon magnetic nanohybrid material synthesized from black cumin (Nigella sativa) industrial processing wastes for lead removal," *Biomass Conv. Bioref*, vol. 15, pp. 10917–10932, Jul. 2024, doi: 10.1007/s13399-024-05910-w.

[7] W. Jing et al, "$MnFe_2O_4$-loaded bamboo pulp carbon-based aerogel composite: synthesis, characterization and adsorption behavior study for heavy metals removal," *RSC Adv.*, vol. 14, pp. 39995–40005, Dec. 2024, doi: 10.1039/D4RA06363E.

[8] G. Vatankhah, F. Parsa, D. Jafari et al, "Evaluation of adsorptive performance of Mn-doped Fe_2O_4 nanoparticles loaded on activated carbon in removal of boron ions from synthetic wastewater," *Biomass Conv. Bioref*, vol. 14, pp. 26477–26487, Aug. 2023, doi: 10.1007/s13399-023-04695-8.

[9] P. T. Lan Huong et al., "Functional manganese ferrite/graphene oxide nanocomposites: Effects of graphene oxide on the adsorption mechanisms of organic MB dye and inorganic As(v) ions from aqueous solution," *RSC Adv.*, vol. 8, no. 22, pp. 12376–12389, 2018, doi: 10.1039/c8ra00270c.

[10] N. N. Thinh et al., "Magnetic chitosan nanoparticles for removal of Cr(VI) from aqueous solution," *Mater. Sci. Eng*. C, vol. 33, no. 3, pp. 1214–1218, Apr. 2013, doi: 10.1016/j.msec.2012.12.013.

[11] M. A. M. Taguba et al., "Nonlinear Isotherm and Kinetic Modeling of Cu(II) and Pb(II) uptake from water by $MnFe_2O_4$/Chitosan Nanoadsorbents," *Water*, vol. 13, pp. 1662, 2021, doi: 10.3390/w13121662.

[12] A.T. Puari, R. Rusnam, N.R. Yanti, M.Y. Shukor, "Adsorption Performance of Biochar From Exhausted Coffee Husk (ECH) Under Various Carbonization Parameters on Copper (II) Ion in Aqueous Solution," *Iop Conf. Ser. Earth Environ. Sci*. vol. 1426, pp 12011, Dec. 2024, doi: 10.1088/1755-1315/1426/1/012011.

[13] A.L.F. de C. Melo, M.T. Carneiro, A.M.S.S. Nascimento, A.Í.S. Morais, R.D.S. Bezerra, B.C. Viana, J.A. Osajima, E.C. Silva-Filho, "Biochar Obtained From Caryocar Brasiliense Endocarp for Removal of Dyes From the Aqueous Medium," *Materials (Basel).* vol. 15, pp. 9076, Dec. 2022, doi: 10.3390/ma15249076.

[14] P. Wang, M. Stenrød, L. Wang, S. Yuan, L. Mao, L. Zhu, L. Zhang, Y. Zhang, H. Jiang, Y. Zheng, X. Liu, "Characterization of Montmorillonite–Biochar Composite and Its Application in the Removal of Atrazine in Aqueous Solution and Soil", *Front. Environ. Sci.*, vol. 10, pp. 888252, 2022, doi: 10.3389/fenvs.2022.888252.

[15] S. Altaf, H. Ajaz, M. Imran, A. Ul – Hamid, M. Naz, M. Aqeel, A. Shahzadi, A. Shahbaz, M. Ikram "Synthesis

and characterization of binary selenides of transition metals to investigate its photocatalytic, antimicrobial and anticancer efficacy," *Applied Nanoscience*, 10, pp. 2113–2127, Mar. 2020, doi: 10.1007/s13204-020-01350-w.

[16] Y. Yang, et al., "ZnO nanoparticles loaded rice husk biochar as an effective adsorbent for removing reactive red 24 from aqueous solution," *Mater Sci Semicond Process,* vol.150, pp. 106960, Nov. 2022, doi: 10.1016/j.mssp.2022.106960.

[17] P. T. L. Huong, N. Tu, H. Lan, L.H. Thang, N. V. Quy, P. A. Tuan, N. X. Dinh, V. N Phan, A. T. Le, "Functional manganese ferrite/graphene oxide nanocomposites: effects of graphene oxide on the adsorption mechanisms of organic MB dye and inorganic As (v) ions from aqueous solution," *RSC Adv,* vol. 8, pp. 12376–12389, 2018, doi: 10.1039/c8ra00270c.

[18] M. Kosmulski, "The pH dependent surface charging and points of zero charge. VII. Update," *Adv. Colloid Interface Sci.*, vol. 251, pp. 115–138, 2018, doi: 10.1016/j.cis.2017.10.005.

[19] K. Mulani, S. Daniels, K. Rajdeo, S. Tambe, and N. Chavan, "Adsorption of Chromium(VI) from Aqueous Solutions by Coffee Polyphenol-Formaldehyde/Acetaldehyde Resins," *J. Polym*., vol. 2013, pp. 1–11, 2013, doi: 10.1155/2013/798368.

[20] T. M. Kazeem, S. A. Lateef, S. A. Ganiyu, M. Qamaruddin, A. Tminu, K. O. Sulaiman, S. M. S. Jilani, and K. Ahooshani, "Aluminum-Modified Activated Carbon as Efficient Adsorbent for Cleaning Cationic Dye in Wastewater," *Journal of Cleaner Production,* vol. 205, pp. 303–312, 2018, doi:10.1016/j.jclepro.2018.09.114.

[21] Ho, Y., "Review of Second-Order Models for Adsorption Systems", *J. Hazard. Mater.,* vol. 136, pp. 681–689, Aug. 2006, doi: 10.1016/j.jhazmat.2005.12.043.

[22] L.H. Nguyen, T.M. Vu, T.T. Le, V.T. Trinh, T.P. Tran & H.T. Van, "Cr(VI) removal from aqueous solutions by fixed-bed column using corncob-based modified biochar," *Enviromental Technology*, vol. 40(6), pp. 683–692, Nov. 2017, doi: 10.1080/09593330.2017.1404134.

[23] Y. C. Sharma and V. Srivastava, *"*Comparative studies of removal of Cr(VI) and Ni(II) from aqueous solutions by magnetic nanoparticles,*"* *J. Chem. Eng. Data*, vol. 56, no. 4, pp. 819–825, Oct. 2010, doi: 10.1021/je100428z.

[24] N. Li, F. Fu, J. Lu, Z. Ding, B. Tang, and J. Pang, "Facile preparation of magnetic mesoporous $MnFe_2O_4$@SiO_2−CTAB composites for Cr(VI) adsorption and reduction," *Environ. Pollut*., vol. 220, pp. 1376–1385, Jan. 2017, doi: 10.1016/j.envpol.2016.10.097.

[25] D. Prabu, P. S. Kumar, B. S. Rathi, S. Sathish, K. V. Anand, et al. "Feasibility of magnetic nano adsorbent impregnated with activated carbon from animal bone waste: application for the chromium (VI) removal," *Environmental Research*, vol. 203, pp. 111813, 2022, doi: 10.1016/j.envres.2021.111813.